

Automatic coral reef fish identification and 3D measurement in the wild

Cyril Barrelet¹, Marc Chaumont^{1,2}, Gérard Subsol¹

1. Research-team ICAR, LIRMM, Univ Montpellier, CNRS, France,

2. Univ Nîmes, France

{cyril.barrelet, marc.chaumont, gerard.subsol}@lirmm.fr

May 2023

1 Introduction

Monitoring marine biodiversity has become essential to track potential species decline or invasive species due to overfishing, pollution, or global warming.

Marine ecologists used to dive underwater and count species on the fly, sometimes estimating their length by eye. As those missions are costly, Computer vision methods have become very promising in this field. While a person can dive for about one hour, multiple underwater cameras can capture video for several hours, resulting in thousands of videos.

Analyzing this material is very time-consuming, and therefore many works have been done to count fishes within videos automatically ([1], [2], [3]).

However, more than counting fish is needed to monitor marine life effectively. Indeed, another indicator is the inter-species biomass, which needs to know the fish species and their length. Acquiring this length is possible with stereoscopic cameras through a camera calibration process.

VidSync [4] is a software that helps marine ecologists calibrate cameras and measure fish manually within a video. An operator must select points in both left and right images and get a 3D measurement thanks to the calibration of the camera.

This method is tedious, considering the number of videos, and it is prone to error since the operator also has to identify the species.

Many works were interested in fish detection ([5], [6], [7], [8]), species identification ([9], [10]), and fish movement tracking ([11], [12], [13]) on mono cameras, while a few worked on stereo cameras ([14], [15]). None of them have since automatically detected, identified, measured, and tracked fish in wild underwater environments.

Thus, this paper introduces an automatic 3D fish population analysis pipeline within wild underwater videos.

2 Materials and Methods

2.1 Method overview

As our automatic 3D fish analysis procedure flowchart shows in Figure 13, the very first blocs consist in getting stereo videos.

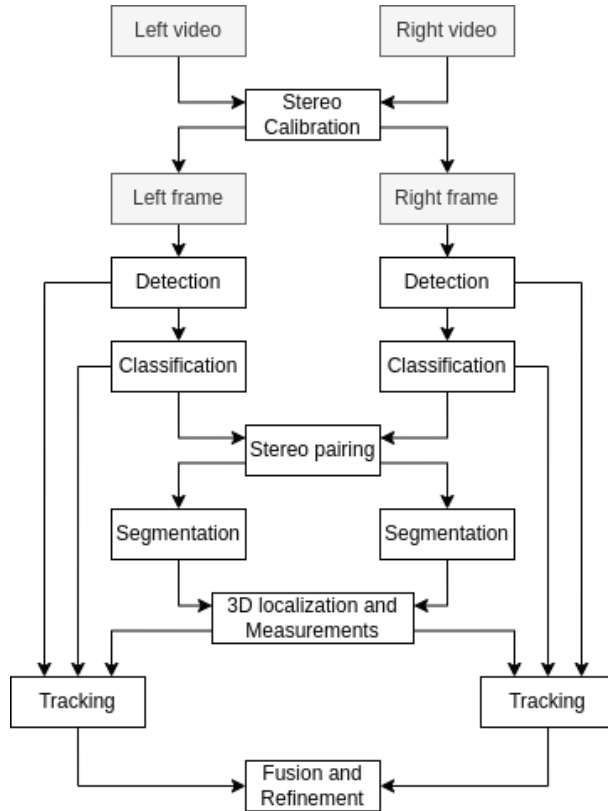


Figure 1: **Flowchart** Our automatic 3D fish population analysis pipeline.

Hence, we first recorded videos in various environments with a stereoscopic camera system, as shown in Figure 2, which consists of two GoPro¹ Hero 4 cameras with a resolution of 1080×1920 , both housed in a diving case, fixed on a rigid rig 80 cm apart. Since both cameras need to be synchronized, we attached a blinking LED in front of each camera view, allowing for manual synchronization and preventing future divergence in the caption.

We summarize the pipeline as follows:

- **Calibration:** From the left V_L and right V_R videos, we estimate the parameters of the cameras through a calibration procedure, detailed in section 2.2.

¹<https://gopro.com>



Figure 2: **Our stereo system** Two GoPro Hero 4 cameras fixed on a rigid rig.

- **Detection:** Independently, each left I_L and right I_R image passes through our fish detection model, explained in section 2.3, acquiring the 2D localization of the detected fish through their corresponding bounding boxes BB in both images.
- **Classification:** The thumbnail of every detected left BB_L and right BB_R bounding box passes then through our species classification model, presented in section 2.4, identifying the species of every fish.
- **Stereo pairing:** We rectify I_L and right I_R knowing the calibration parameters, allowing to pair, as described in section 2.5, each BB_L to their corresponding BB_R .
- **Segmentation:** Paired thumbnails pass through our fish segmentation model, presented in section 2.6, allowing us to create a pixel-wise mask of both left and right fish.
- **3D localization and measurement:** Given the paired masks of every fish, we localize the 2D position of their snout and tail and measure their corresponding 3D position, allowing us to get their size and 3D localization in the camera space, as explained in section 2.7.
- **Tracking:** We track the fish as long as they appear in the image, keeping their 2D and 3D positions and their top-5 species identification, as clarified in section 2.8.
- **Fusion and refinement:** Finally, we associate the same fish's left and right tracks, allowing for the smoothing of both the measurements and identification as described in section 2.9.

2.2 Calibration

The camera calibration is a procedure allowing us to estimate cameras' parameters, distortion coefficients, and their relative position and orientation from one another.

By triangulation, it gives the ability to measure the distance between a point and the camera coordinate system noted $O_{L,R}$ in Figure 3.

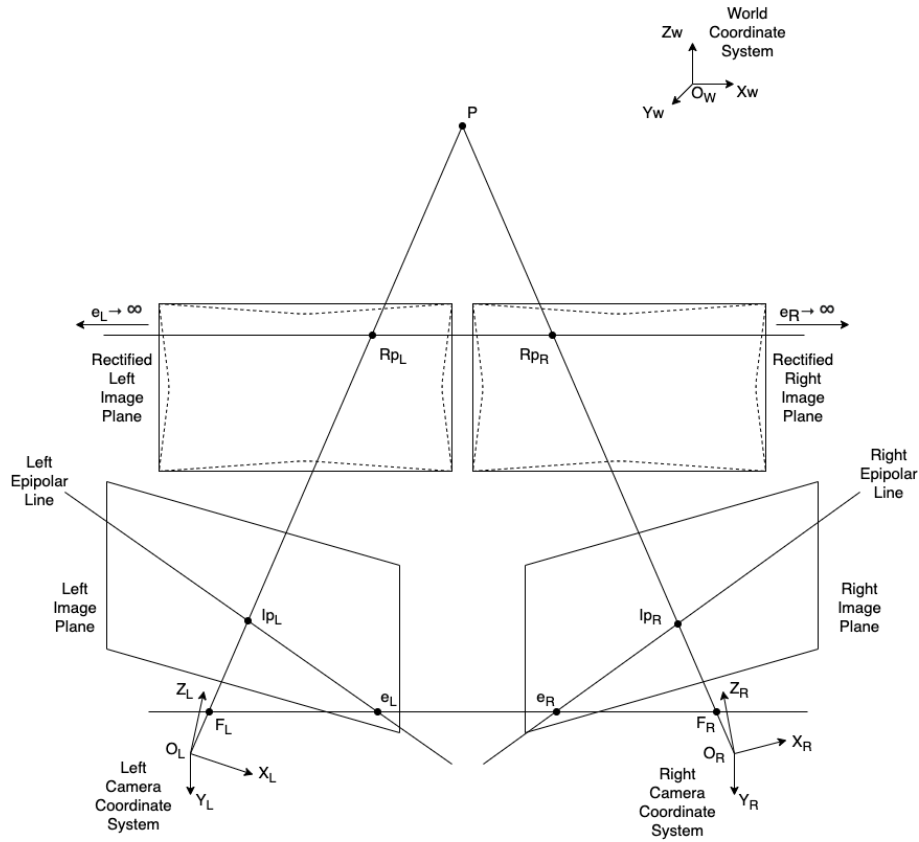


Figure 3: **Epipolar geometry** Rectification scheme.

METHOD

After arriving at each dive location, the first step is to move a calibration pattern with known dimensions in front of the stereo cameras. As we will discuss later, different calibration pattern forms exist. Though, we used the calibration pattern generator from the OpenCV² library [16] for the sake of simplicity.

Given that the cameras are synchronized, meaning the first frame of one camera is temporally related to the first frame of the other one, the second step is to select 20 - 30 stereo frames, $I_L^{t_n}$ and $I_R^{t_n}$, manually where both cameras can see the calibration pattern.

The final and automatic step is estimating, for each camera, their parameters, their

²OpenCV: <https://opencv.org/>

distortion coefficient, and their relative position and orientation from one another. The camera parameters form a so-called projection matrix of size 3×4 , composed of the intrinsic and extrinsic parameters, as shown in (1).

$$\begin{bmatrix} u \\ v \\ 1 \end{bmatrix} = \begin{bmatrix} f_x & 0 & c_x \\ s & f_y & c_y \\ 0 & 0 & 1 \end{bmatrix} \begin{bmatrix} r_{11} & r_{12} & r_{13} & t_x \\ r_{21} & r_{22} & r_{23} & t_y \\ r_{31} & r_{32} & r_{33} & t_z \end{bmatrix} \begin{bmatrix} X_w \\ Y_w \\ Z_w \\ 1 \end{bmatrix} \quad (1)$$

The intrinsic parameters link the pixel coordinate of an image point with the corresponding coordinate in the camera space. These consist of its focal length in mm, noted f_x and f_y , its optical center in pixel, noted c_x and c_y , and its skew coefficient, noted s , defining the angle between the x and y pixel axes.

The extrinsic parameters describe the position and orientation of the camera in the world. These consist of a rotation matrix of size 3×3 noted r_{ij} and a translation matrix of size 3×1 noted $t_{x, y, z}$.

As shown in equation (1), the projection matrix allows transforming a 2D system coordinate, noted u and v , to a 3D world system coordinate noted X_w , Y_w , and Z_w .

Using those previously selected stereo frames and the OpenCV library implementation of Bouget's Calibration Toolbox³ inspired by Zhang's technique [17], we can automatically detect the calibration pattern corners, thanks to the Harris Corner Detector [18], and extract the described camera parameters and the distortion coefficients for each camera. Then, we can estimate the relative position and orientation from the left to the right camera with the coordinates' corners set, the cameras' parameters, and the distortion coefficients.

Given those calibration parameters, we correct the lens distortions and rectify the images.

As shown in Figure 4, the conjunction of the two focal points F_R and F_L of the right and left camera respectively intersects I_L and I_R in two specific points, e_L and e_R , called left and right epipoles, respectively [19]. If I_{pR} is the projection of the generic point P of the scene into I_R , its corresponding point I_{pL} in I_L has to be searched for on the left epipolar line obtained connecting I_{pL} with the left epipole. The rectification is an image transformation that makes the epipolar lines collinear with the image scan lines; thus, the epipoles are shifted to infinity.

In other words, finding correspondence between each right R_{pR} rectified image pixel and its matching left R_{pL} rectified image pixel only requires searching in a unique axis along the epipolar lines, as shown in Figure 4. It is called the epipolar constraint.

PRACTICAL CASE

We printed a checkerboard with 5×8 tiles of 5 cm as the calibration pattern and plasticized it on a rigid board.

³Bouget's Calibration Toolbox: <http://www.vision.caltech.edu/bouguetj/calib>

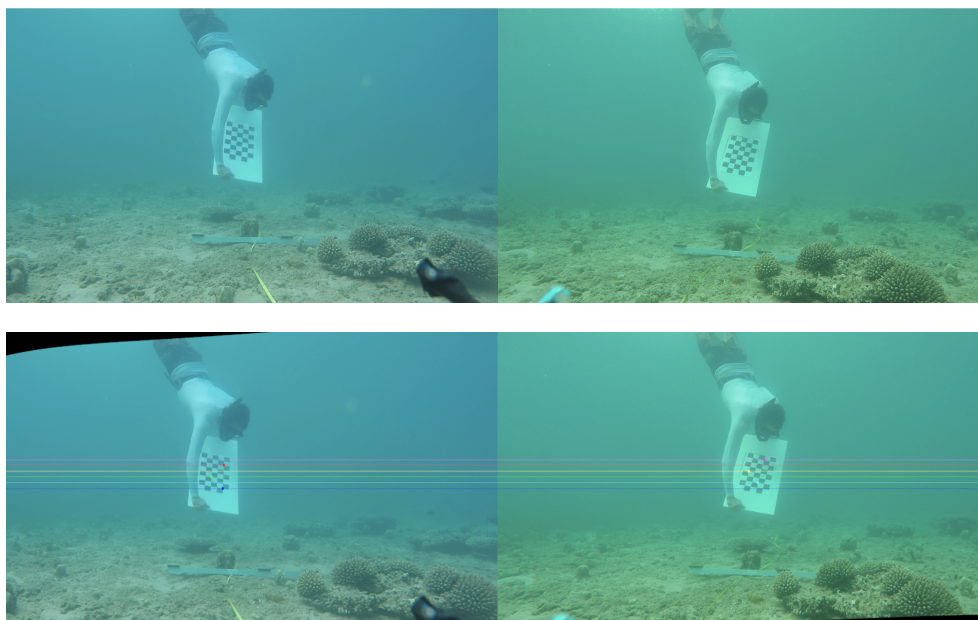


Figure 4: **Image rectification** (Top) The original stereo frames with the calibration pattern. (Bottom) The same stereo frames but rectified.

Then, we recorded a diver holding the board at various positions and orientations within 1 - 3 m from the stereo cameras rig.

Secondly, we manually synchronized V_L and V_R thanks to the blinking LEDs and a clap that the diver did as a reference at the beginning of the recording.

Finally, we manually extracted 20-30 frames in which the calibration pattern could be detected in both I_L and I_R .

Then, we give those images to the calibration algorithm doing the rest automatically.

2.3 Detection

We train an object detection neural network to detect and localize fish within the images, as shown in the detection block of Figure 13. Many object detection neural networks exist: R-CNN [20], Fast R-CNN [21], YoloV3 [22], or YoloV4 [23], for instance. We chose YoloV5 [24] which is very efficient.

Once trained, the model estimates Bounding Boxes, BBs, at the fish location according to a threshold. This threshold allows retaining every BB whose confidence score, given by the regression, is not under it. We kept this threshold according to the original YOLOv5 implementation.

YOLOv5 can detect and identify an object simultaneously. However, it does not manage class balancing within the identification task, and since our fish detection database B_{det} is poorly balanced, we get around this problem indirectly. Hence, we deliberately separate the localization from the identification task, allowing YOLOv5 to detect only

fish-looking objects.

FISH DETECTION DATABASE

Our B_{det} consists of 3,362 manually annotated frames, with between 0 to 34 fish, extracted from various videos in shallow water taken in Mayotte and Scattered Islands at different times, for a total of 32,054 annotated BBs.

Additionally, every fish were identified. Every species has an average of 204 BBs but a standard deviation of 923 BBS because the number of BBs per species ranges from 1 to 10,675, as shown in Table 1 (Supplementary materials).

We randomly split the database into a train, a validation, and a test set with a ratio of 80-10-10, respectively.

DATA AUGMENTATION

Indeed, underwater images suffer from turbidity, color distortion, and low contrast because the light is attenuated while it propagates through water [25].

As more than the size of our database is needed to obviate those problems and to generalize the detection for every case, we use data augmentation techniques.

Thus, we performed color space and geometric transformations. We randomly apply a horizontal flip and modify the contrast within a range of 60 to 140% [26].

METHOD AND PARAMETERS

As we want YOLOv5 to detect only fish-looking objects, we set the number of classes to one. We chose the YOLOv5x6 model pre-trained on ImageNet at a resolution of 1280×1280 pixels. From its pre-trained weights, we used transfer learning to keep the previous knowledge. We chose the SGD optimizer and kept the same settings from the YOLOv5 V5.0 version. Finally, we set the batch size at four, the maximum according to our GPU capability (NVIDIA⁴ Quadro RTX 6000 with 24Go VRAM). We also investigated the batch size and resolution influence on different YOLOv5 models in the Supplementary material section.

Finally, we obtained a Precision of 82.9% and a Recall of 84.7%, with a mAP@.5 of 87.7% on the test set. Figure 5 shows the result of the detection.

2.4 Classification

The classification aims to train a Convolutional Neural Network for fish species identification. Once a fish is detected, its BB is cut out from the image. Then, this thumbnail passes through the neural network that gives us the logistic regression and hence its species and a confidence score.

As examples are needed to train a CNN, we used a species identification database.

⁴<https://www.nvidia.com/>



Figure 5: A frame where each fish-looking object is detected while specifying the confidence score YoloV5 attributes.

SPECIES IDENTIFICATION DATABASE

Our species identification database B_{id} contains 56 different species classes and heights environmental classes such as algae or coral, as listed in Table 2 (Supplementary materials). Each class consists of ($n=64$) $2,757.6 \pm 1,844.8$ thumbnails with diverse sizes manually extracted from various videos with the same conditions that our B_{det} but at a different period, for a total of 44,625 annotated thumbnails. As we did for the fish detection task, we split this database into three datasets respecting the same ratio.

DATA AUGMENTATION

To help generalize, we also used the same augmentation techniques mentioned before. In addition, to prevent erroneous identification due to the occlusion problem within the fish detection task, we added 56 new classes representing species parts [27] to our database, which now has 120 different classes. Thus, we cut vertically and horizontally every species thumbnail while considering class balancing.

METHOD AND PARAMETERS

We selected the EfficientNet-B6 model [28], which has 46M parameters, with slightly different settings from the original paper: ADAM optimizer with decay 0.9; batch norm momentum 0.99; weight decay 10^{-5} ; dropout ratio 0.5; initial learning rate 10^{-3} ; the cross-entropy loss function; and a batch size of 16.

Since species identification is challenging, we adopt a two-stage learning approach [29]. First, we only trained its classifier using transfer learning from the ImageNET pre-trained model while freezing all other layers. We dynamically decreased the initial learning rate by 0.1 whenever the validation loss plateaus according to a 'patience' number of epochs.

Then, using fine-tuning, we unfroze all the layers and retrain the entire model. To retain

previous knowledge and avoid forgetting during the fine-tuning, we dropped the initial learning rate to 10^{-4} , decreasing it throughout the training similarly.

Additionally, we set an Early Stopping for both phases, allowing to stop training when parameter updates no longer improve the validation set since large models cannot overfit [30].

We obtained a 97.95% top-5 accuracy after the fine-tuning phase on the test set. Given that the accuracy is nearly perfect, we assumed a possible no mismatch within our B_{id} . Thus, we further tested the model on our B_{det} , as the two databases were created at different times. As expected, we obtained a slightly lower performance reaching a 95.3% top-5 accuracy on B_{det} .

The result of the classification is shown in Figure 6. Since we can detect and identify fish in the stereo pair, we propose a method to associate every BB from I_L , BB_L , to their corresponding BB on I_R , BB_R .

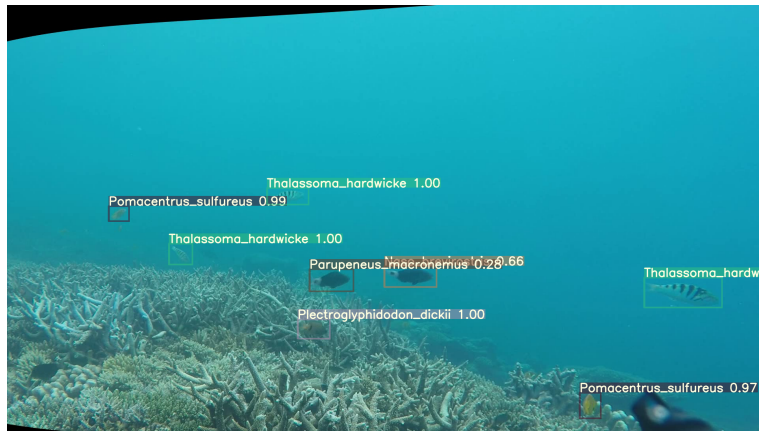


Figure 6: A frame where each BB is identified while specifying the confidence score EfficientNet attributes. The two central fish identified as *Parupeneus macronemus* and *Naso brevirostris* have a low confidence score, which suggests erroneous identification. This species is, in fact, not part of B_{id}

2.5 Stereo pairing

While we need to find correspondence between pixels from I_L and I_R , even though we only look on one axis thanks to the image’s rectification, this pixel matching could be misleading. Indeed, as we need to go through every pixel across the epipolar line to find correspondence, faulty matching could occur, resulting in an incorrect measurement. Thus, we proposed a method for matching left and right BBs, allowing robust pixel-level matching.

METHOD AND ALGORITHM

Firstly, for each BB_L and BB_R , we extract their 1×2316 dimension vector from the Global Average Pooling layer of the EfficientNet’s feature extractor. Since this feature vector is previous to the classification network, as shown in Figure 7, it is a thin-grained image representation of the species. Thereby, we can use it as a similarity metric.

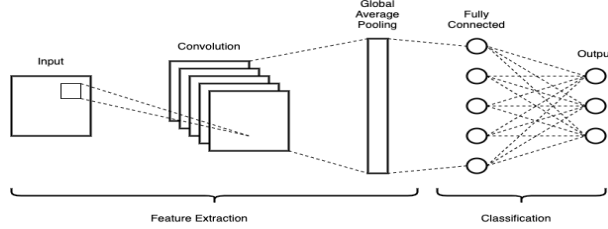


Figure 7: Schematic diagram of a basic CNN

Secondly, for each center coordinate of BB_{S_L} , we look for all center coordinates of BB_{S_R} along the same epipolar line within a delta of five pixels. Moreover, we compute the Cosine similarity between their feature vector, giving an appearance distance.

Lastly, we define a bipartite graph consisting of two independent sets U and V , respectively BB_{S_L} and BB_{S_R} IDs. Then, we set the edges and weights accordingly to the previous steps, as shown in Figure 8.

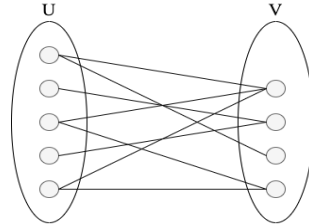


Figure 8: **Bipartite graph:** BB_{S_L} IDs on the left and BB_{S_R} IDs with their respective cosine similarity as weights.

Finally, we solve this one-to-one pairing optimization problem using the Hungarian algorithm [31], maximizing the sum of the weights.

Given that we do not have any available database to measure our method’s performance yet, we tested it visually on a few stereo-pair images and assumed it works reasonably.

As shown in Figure 9, each paired BB share the same color, and their Id is complementary. The red-colored BBs mean that we could not find any stereo correspondence. Then, we need to segment all pixels that belong to the fish to determine the snout and tail positions.

Then, we need to segment all pixels that belong to the fish to determine the snout and tail positions.



Figure 9: Left and right frame highlighting paired BBs with the same color and complementary ID. Red-colored BBs indicate that there is no correspondence.

2.6 Segmentation

The segmentation allows for finding a binary mask of the fishes in order to determine their contours. Like detection and classification, a semantic image segmentation network, such as Mask-RCNN [32], EfficientNet-L2 [33] or GoogleDeepLabv3+ [34], has to be trained with examples. We chose the GoogleDeepLabv3+ implementation, which performs well on many tasks.

As segmentation takes some time and is unnecessary when a fish is not paired, hence, we only segmented paired fish to reduce the computation time.

Once a fish is paired on both I_L and I_R , their BB is cut out from the images. Then, these two cutouts pass through the segmentation network, which gives two binary masks, M_L and M_R , for the same fish detected on I_L and I_R .

Given that no fish segmentation was available, we created a small database.

FISH SEGMENTATION DATABASE

From B_{id} , we built our fish segmentation database B_{seg} by randomly selecting 25 thumbnails per species for 1,600 thumbnails. First, we enlarged each thumbnail and manually drew a polygon on the fish edges. Next, the previously drawn mask is rescaled to the original thumbnail size.

Considering that our B_{seg} is relatively small, we segment fish-looking objects rather than species. Finally, we split B_{seg} into three different datasets respecting the same ratio as we did for detection and classification.

METHOD AND PARAMETERS

As mentioned, we selected the DeepLabv3+ model with a ResNet-101 [35] backbone pre-trained on ImageNet. We used the same parameters from the original paper: SGD optimizer; batch norm momentum 0.9; weight decay 10^{-5} ; initial learning rate 10^{-4} , a

learning rate policy where the learning rate is multiplied by $(1 - \frac{iter}{maxiter})^{0.9}$; the cross entropy loss function; and a batch size of 8. Additionally, we used an Early Stopping for the same reasons explained in the classification part. Finally, we obtained a mIoU of 84.4% on the test set.

The result of the segmentation is shown in Figure 10.



Figure 10: Shows the fish detection, identification, and, when BBs are paired, segmentation.

2.7 3D localization and measurements

To establish the snout and the tail, but also the bottom and the upper part positions from the fish, we first find the extreme points of M_L and M_R , namely the sets P_L and P_R , by determining the principal axis of inertia using a PCA, as shown in Figure 11. b).

Then, we project the set P_L on M_R using epipolar constraint, within a 3 pixels delta on the y axis, to find left to right correspondences P_{LR} , as shown in Figure 11. c). Given that M_L and M_R could be different, we repeat the same process to find right-to-left correspondences P_{RL} from M_R to M_L , as shown in Figure 11. d).

Finally, we compute 3D point coordinates by triangulation using the projection matrices of the cameras for P_{LR} and P_{RL} . Therefore, we estimate the Fork length of the fish and its height for P_{LR} and P_{RL} by computing the Euclidean distances.

Because of the direction, we have two measurements for the length and the height. Therefore, we chose to take the mean of the lengths and the heights.

Additionally, we compute the barycenter for the sets P_L and P_R , respectively, the points B_L and B_R . As we did for the length and the height, we find the left-to-right barycenter correspondence set B_{LR} by taking the point B_L and creating its correspondent point as $B_{R'} = (B_{R_x}, B_{L_y})$.

Moreover, we find the right to left correspondence $B_{RL} = \{B_R; B_{L'}=(B_{L_x}, B_{R_y})\}$. Finally, we compute the 3D coordinates of the center for the sets B_{LR} and B_{RL} and take the mean between those two points. Figure 12 shows the result of the measurement.

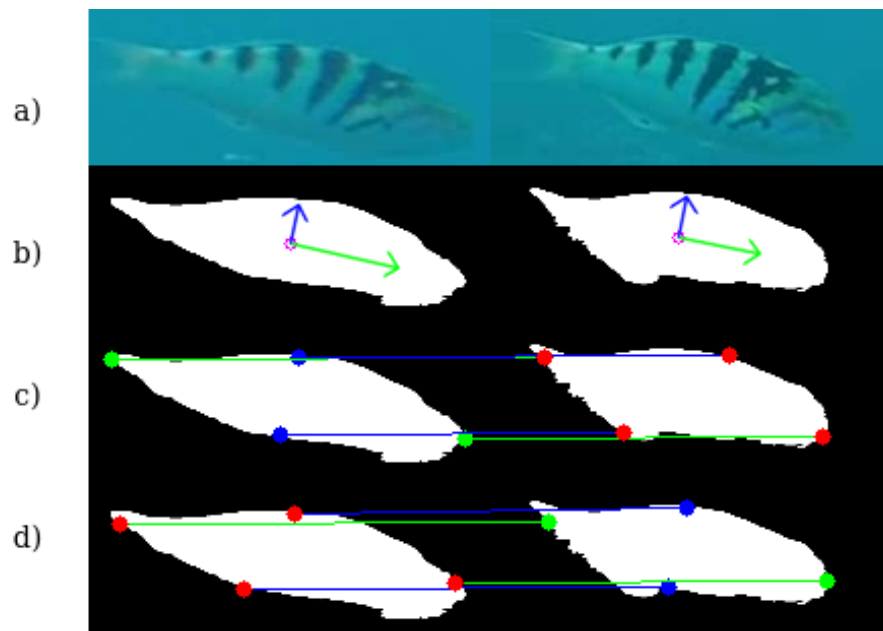


Figure 11: Measurements points determination: a) Paired left and right fish; b) PCA on M_L and M_R ; c) Projection of the set P_L , represented in green and blue dots, on M_R to obtain left to right corresponding points represented in red.; d) Projection of the set P_R , represented in blue and red dots, on M_L to obtain right to left corresponding points represented in red.

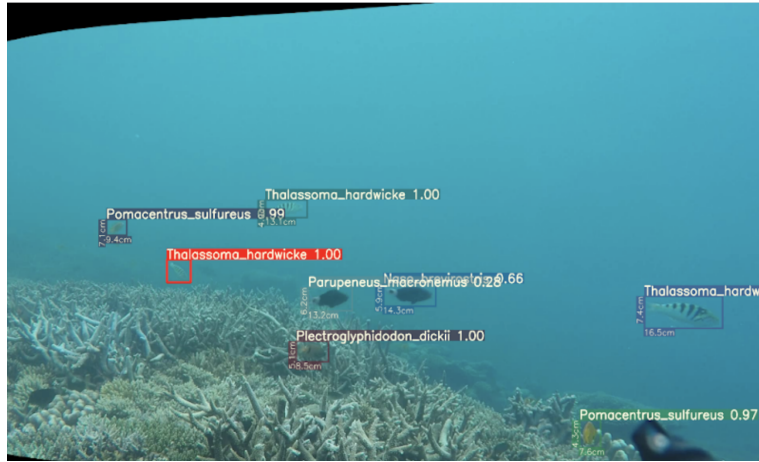


Figure 12: Shows the fish detection, identification, and measurement.

2.8 Tracking

Ultimately, we added Multi-Object tracking to the pipeline to make it more robust. This addition enables us to track every BB over time, even though some detections miss. We used DeepSORT [36], based on SORT [37] to keep track of every detected fish on V_L , and V_R .

For each $BB_{L_i}^{t_n}$ on $I_L^{t_n}$, a new tracker is made, and is set as tentative. The tracker is enabled when the IoU between $BB_{L_i}^{t_n}$ and $BB_{L_i}^{t_{n+1}}$ is greater than a threshold for $n = \{0; 1; 2\}$.

Secondly, the motion model is built according to a standard Kalman filter with constant velocity and a linear observation model where the BB coordinates and aspect ratio are taken as direct observation of the object state. DeepSORT uses the squared Mahalanobis distance between predicted Kalman states and newly arrived measurements to assign a new BB to an existing tracker. However, the Mahalanobis distance is a uniform metric for tracking through occlusions.

Therefore, a second metric is integrated into the assignment problem. Finally, DeepSORT keeps a gallery of each track's last 100 associated appearance descriptors. We set this appearance descriptor to the feature vector we extracted from the classifier. Then, the second metric measures the smallest cosine distance between the $BB_{L_i}^{t_n}$ and the whole gallery.

Next, DeepSORT builds the association problem by combining metrics with a weighted sum and solves the problem by introducing a matching cascade considering the association likelihood.

Finally, we repeat the process for each $BB_{R_i}^{t_n}$ on $I_R^{t_n}$, allowing us to track every classification and, when possible, measurements for the same fish through its appearance in the video.

2.9 Fusion and refinement

While a fish can be identified and measured automatically, errors could occur through classification and segmentation. To alleviate those issues, we chose to take advantage of the tracking to smooth the results.

First, we associate each left track with its corresponding right track, considering that both left and right fish should be paired in the same time frame. Therefore, we have a unique track for recording left and right classifications and measurements.

Secondly, we sum up the classification top-5 score each time a fish is identified and retain the most likely identification for each unique track.

Additionally, we chose to take the median of all measurements for the length and height.

3 Results

Our method yields a multifaceted range of results due to its comprehensive capabilities. The initial 2D positional localization attained through the detection module serves as a foundation for temporal fish enumeration. Furthermore, by incorporating species identification via the classification module, we achieve a comprehensive assessment of piscine diversity.

The segmentation module, when applied, facilitates an in-depth analysis of the morphological characteristics of various species. It allows for an examination of species-specific shapes and structures, thus offering a more nuanced understanding of the aquatic fauna. Additionally, the integration of 3D positional localization, coupled with segmentation data, enables accurate estimations of fish sizes. This information, coupled with species identification and population dynamics over time, allows for the calculation of biomass within the ecosystem.

Furthermore, our method’s ability to track individual fish across a video sequence enables a thorough analysis of their kinematic aspects. This includes the speed, acceleration profiles, and trajectories, visualized in Figure 13. Additionally, the system provides opportunities to study intra-species interactions and behavioral patterns.

4 Discussion

While we present an automatic fish measurement and identification pipeline, every block could be improved separately.

As detection is challenging in underwater images, we could augment B_{det} with new examples. However, since annotation is time-consuming, we could use recent semi-supervised learning techniques [38], [39], and [40]. While having just a few annotated examples, we have thousands of underwater video records. The semi-supervised learning approach creates new examples from unlabeled data and is proven to improve generalization.

Given that the classifier will always classify whether or not the input is part of the database, the unseen classification object is an open issue. We could set a threshold to class a classification from correct to uncertain [41].

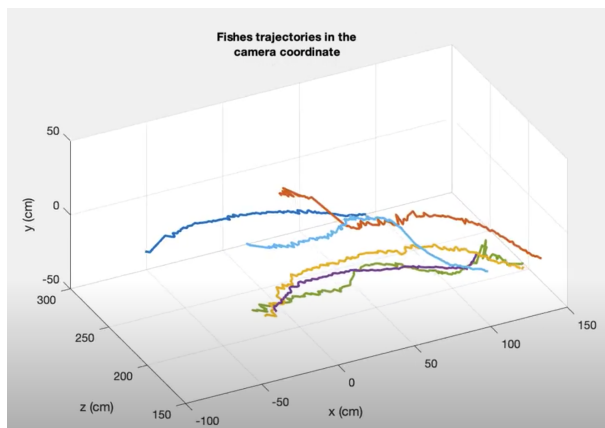


Figure 13: **3D trajectories** Shows captured 3D fish trajectories for a short period of time, where each color represents a different fish.

While the mIoU seems conclusive on the test set for the segmentation, the generalization still needs to be proven. We could build a more extensive database to improve the segmentation and use weakly supervised techniques. For instance, Puzzle-CAM [42] uses the class activation map of the classification network with a puzzle method to create new examples. Weakly supervised learning could make use of the whole B_{id} , and therefore, improve the generalization.

While PCA is a decent method to find the snout and the tail position, it requires excellent fish segmentation. Moreover, even though the segmentation is good enough, some fish could be taller than long. In that case, we could use a CNN to determine those positions similarly to DeepFish [43], which finds the fish’s center position using points annotation examples. The tracking component could also be improved by using recent online tracking as STGT [44] or by using offline tracking methods [45] and [46]. Nevertheless, since we work on stereo images, we could also integrate the 3D information into the tracking [47].

Acknowledgments

This work was publicly funded through ANR (the French National Research Agency) under the “Investissements d’avenir” program (PIA) with the reference ANR-16-IDEX-0006

Authors’ contributions

All authors conceived the ideas and designed the methodology; J.S.G. led the writing of the manuscript. All authors contributed critically to the drafts and gave final approval for publication.

Conflict of Interest statement

Authors have no conflict of interest to declare.

References

- [1] Y. H. Toh, T. M. Ng, and B. K. Liew, “Automated fish counting using image processing,” in *2009 International Conference on Computational Intelligence and Software Engineering*, 2009, pp. 1–5.
- [2] Ryan Fier, Alexandra Branzan Albu, and Maia Hoeberechts, “Automatic fish counting system for noisy deep-sea videos,” in *2014 Oceans - St. John’s*, 2014, pp. 1–6.
- [3] Geoffrey French, Mark Fisher, Michal Mackiewicz, and Coby Needle, “Convolutional neural networks for counting fish in fisheries surveillance video,” 09 2015.
- [4] Jason Neuswanger, Mark Wipfli, Amanda Rosenberger, and Nicholas Hughes, “Measuring fish and their physical habitats: Versatile 2-d and 3-d video techniques with user-friendly software,” *Canadian Journal of Fisheries and Aquatic Sciences*, vol. 73, 06 2016.
- [5] Sébastien Villon, Marc Chaumont, Gérard Subsol, Sébastien Villéger, Thomas Claverie, and David Mouillot, “Coral reef fish detection and recognition in underwater videos by supervised machine learning : Comparison between Deep Learning and HOG+SVM methods,” in *ACIVS: Advanced Concepts for Intelligent Vision Systems*, Lecce, Italy, Oct. 2016, vol. Image Processing, Computer Vision, Pattern Recognition, and Graphics, Springer.
- [6] Suxia Cui, Yu Zhou, Yonghui Wang, and Lujun Zhai, “Fish detection using deep learning,” vol. 2020, pp. 3738108, Publisher: Hindawi.
- [7] Rekha B S, Dr. Srinivasan G N, Sravan Reddy, Divyanshu Kakwani, and Niraj Bhattad, *Fish Detection and Classification Using Convolutional Neural Networks*, pp. 1221–1231, 01 2020.
- [8] Youssef Wageeh, Hussam El-Din Mohamed, Ali Fadl, Omar Anas, Noha ElMasry, Ayman Nabil, and Ayman Atia, “YOLO fish detection with euclidean tracking in fish farms,” vol. 12, no. 1, pp. 5–12.
- [9] Ariel G. Cabreira, Martín Tripode, and Adrián Madirolas, “Artificial neural networks for fish-species identification,” vol. 66, no. 6, pp. 1119–1129, eprint: <https://academic.oup.com/icesjms/article-pdf/66/6/1119/29132907/fsp009.pdf>.
- [10] Sebastien Villon, Corina Iovan, Morgan Mangeas, Thomas Claverie, David Mouillot, Sébastien Villéger, and Laurent Vigliola, “Automatic underwater fish species classification with limited data using few-shot learning,” *Ecological Informatics*, vol. 63, pp. 101320, 05 2021.

- [11] Ekram Hossain, S. M. Shaiful Alam, Amin Ahsan Ali, and M Ashraf Amin, “Fish activity tracking and species identification in underwater video,” in *2016 5th International Conference on Informatics, Electronics and Vision (ICIEV)*, 2016, pp. 62–66.
- [12] Ramil Lumauag and Marevic Nava, “Fish tracking and counting using image processing,” 11 2018, pp. 1–4.
- [13] Sebastian Lopez-Marcano, Eric Jinks, Christina Buelow, Christopher Brown, Dadong Wang, Branislav Kusy, Ellen Ditria, and Rod Connolly, “Automatic detection of fish and tracking of movement for ecology,” 03 2021.
- [14] Meng-Che Chuang, Jenq-Neng Hwang, Kresimir Williams, and Richard Towler, “Tracking live fish from low-contrast and low-frame-rate stereo videos,” *IEEE Transactions on Circuits and Systems for Video Technology*, vol. 25, no. 1, pp. 167–179, 2015.
- [15] Daniel Pérez, Francisco J. Ferrero, Ignacio Alvarez, Marta Valledor, and Juan C. Campo, “Automatic measurement of fish size using stereo vision,” in *2018 IEEE International Instrumentation and Measurement Technology Conference (I2MTC)*, 2018, pp. 1–6.
- [16] G. Bradski, “The OpenCV Library,” *Dr. Dobb’s Journal of Software Tools*, 2000.
- [17] Z. Zhang, “A flexible new technique for camera calibration,” vol. 22, no. 11, pp. 1330–1334.
- [18] C. Harris and M. Stephens, “A combined corner and edge detector,” in *Proceedings of the Alvey Vision Conference 1988*. pp. 23.1–23.6, Alvey Vision Club.
- [19] Paolo Zicari, “Efficient and high performance FPGA-based rectification architecture for stereo vision,” vol. 37, no. 8, pp. 1144–1154.
- [20] Ross Girshick, Jeff Donahue, Trevor Darrell, and Jitendra Malik, “Rich feature hierarchies for accurate object detection and semantic segmentation,” .
- [21] Ross Girshick, “Fast r-CNN,” .
- [22] Joseph Redmon and Ali Farhadi, “YOLOv3: An incremental improvement,” .
- [23] Alexey Bochkovskiy, Chien-Yao Wang, and Hong-Yuan Mark Liao, “YOLOv4: Optimal speed and accuracy of object detection,” .
- [24] Glenn Jocher, Alex Stoken, Jirka Borovec, Nano Code, Christopher Stan, Liu Changyu, Laughing, tkianai, Adam Hogan, lorenzomamma, yx Nong, Alex Wang, Laurentiu Diaconu, Marc, wang Haoyang, ml ah, Doug, Francisco Ingham, Frederik, Guilhen, Hatovix, Jake Poznanski, Jiacong Fang, Lijun Yu, changyu, Mingyu Wang, Naman Gupta, Osama Akhtar, PetrDvoracek, and Prashant Rai, “ultralytics/yolov5: v3.1 - Bug Fixes and Performance Improvements,” Oct. 2020.

- [25] Dana Berman, Deborah Levy, Shai Avidan, and Tali Treibitz, “Underwater single image color restoration using haze-lines and a new quantitative dataset,” *IEEE Transactions on Pattern Analysis and Machine Intelligence*, 2020.
- [26] Connor Shorten and Taghi M. Khoshgoftaar, “A survey on image data augmentation for deep learning,” vol. 6, no. 1, pp. 60.
- [27] Sébastien Villon, David Mouillot, Marc Chaumont, Emily S. Darling, Gérard Subsol, Thomas Claverie, and Sébastien Villéger, “A deep learning method for accurate and fast identification of coral reef fishes in underwater images,” vol. 48, pp. 238–244.
- [28] Mingxing Tan and Quoc V. Le, “EfficientNet: Rethinking model scaling for convolutional neural networks,” .
- [29] Jeremy Howard and Sebastian Ruder, “Universal language model fine-tuning for text classification,” in *Proceedings of the 56th Annual Meeting of the Association for Computational Linguistics (Volume 1: Long Papers)*. pp. 328–339, Association for Computational Linguistics.
- [30] Hugo Ruiz, Marc Chaumont, Mehdi Yedroudj, Ahmed Oulad Amara, Frédéric Comby, and Gérard Subsol, “Analysis of the scalability of a deep-learning network for steganography ”into the wild”,” .
- [31] H. W. Kuhn, “The hungarian method for the assignment problem,” vol. 2, no. 1, pp. 83–97.
- [32] Kaiming He, Georgia Gkioxari, Piotr Dollár, and Ross Girshick, “Mask r-cnn,” in *2017 IEEE International Conference on Computer Vision (ICCV)*, 2017, pp. 2980–2988.
- [33] Qizhe Xie, Minh-Thang Luong, Eduard Hovy, and Quoc V. Le, “Self-training with noisy student improves imagenet classification,” in *2020 IEEE/CVF Conference on Computer Vision and Pattern Recognition (CVPR)*, 2020, pp. 10684–10695.
- [34] Liang-Chieh Chen, George Papandreou, Florian Schroff, and Hartwig Adam, “Rethinking atrous convolution for semantic image segmentation,” *CoRR*, vol. abs/1706.05587, 2017.
- [35] Kaiming He, Xiangyu Zhang, Shaoqing Ren, and Jian Sun, “Deep residual learning for image recognition,” in *2016 IEEE Conference on Computer Vision and Pattern Recognition (CVPR)*, 2016, pp. 770–778.
- [36] Nicolai Wojke, Alex Bewley, and Dietrich Paulus, “Simple online and realtime tracking with a deep association metric,” .
- [37] Alex Bewley, Zongyuan Ge, Lionel Ott, Fabio Ramos, and Ben Upcroft, “Simple online and realtime tracking,” in *2016 IEEE International Conference on Image Processing (ICIP)*, 2016, pp. 3464–3468.

- [38] Nhu-Van Nguyen, Christophe Rigaud, and Jean-Christophe Burie, “Semi-supervised object detection with unlabeled data,” 01 2019, pp. 289–296.
- [39] Kihyuk Sohn, Zizhao Zhang, Chun-Liang Li, Han Zhang, Chen-Yu Lee, and Tomas Pfister, “A simple semi-supervised learning framework for object detection,” *ArXiv*, vol. abs/2005.04757, 2020.
- [40] Yen-Cheng Liu, Chih-Yao Ma, Zijian He, Chia-Wen Kuo, Kan Chen, Peizhao Zhang, Bichen Wu, Zsolt Kira, and Peter Vajda, “Unbiased teacher for semi-supervised object detection,” 2021.
- [41] Sébastien Villon, David Mouillot, Marc Chaumont, Gérard Subsol, Thomas Claverie, and Sébastien Villéger, “OPEN a new method to control error rates in automated species,” p. 14.
- [42] Sanghyun Jo and In-Jae Yu, “Puzzle-cam: Improved localization via matching partial and full features,” *2021 IEEE International Conference on Image Processing (ICIP)*, Sep 2021.
- [43] Alzayat Saleh, Issam H. Laradji, Dmitry A. Konovalov, Michael Bradley, David Vazquez, and Marcus Sheaves, “A realistic fish-habitat dataset to evaluate algorithms for underwater visual analysis,” vol. 10, no. 1, pp. 14671.
- [44] Peng Chu, Jiang Wang, Quanzeng You, Haibin Ling, and Zicheng Liu, “Transmot: Spatial-temporal graph transformer for multiple object tracking,” 2021.
- [45] Seyed Hamid Rezatofighi, Anton Milan, Zhen Zhang, Qinfeng Shi, Anthony Dick, and Ian Reid, “Joint probabilistic data association revisited,” in *2015 IEEE International Conference on Computer Vision (ICCV)*, 2015, pp. 3047–3055.
- [46] Fuxin Li, Arridhana Ciptadi, and James Rehg, “Multiple hypothesis tracking revisited,” 12 2015, pp. 4696–4704.
- [47] Peiliang Li, Xiaozhi Chen, and Shaojie Shen, “Stereo r-cnn based 3d object detection for autonomous driving,” 2019.

Supplementary Materials

Species	Number of thumbnails
Abudefduf	5
Abudefduf sexfasciatus	27
Abudefduf sparoides	102
Abudefduf vaigiensis	62
Acanthurus	86
Acanthurus dussumieri	172
Acanthurus fowleri	7

Species	Number of thumbnails
Acanthurus leucosternon	55
Acanthurus nigricans	11
Acanthurus thompsoni	285
Aethaloperca rogae	99
Aethaloperca rogae juv	7
Amanses scopas	58
Amblyglyphidodon indicus	33
Amphiprion	46
Amphiprion latifasciatus	40
Amphiprion sandaracinos	49
Anampses twistii	16
Aphareus furca	17
Apogonidae	8
Apolemichthys trimaculatus	5
Arothron	97
Arothron nigropunctatus	30
Balistapus	8
Balistapus undulatus	109
Balistidae	5
Bodianus anthioides	8
Bodianus axillaris juv	7
Bodianus diana	11
Caesio lunaris	39
Caesio teres	179
Canthigaster valentini	11
Carangidae	28
Carangoides	4
Caranx melampygus	5
Carcharhinus melanopterus	7
Centropyge	5
Centropyge multispinis	83
Cephalopholis argus	61
Cephalopholis juv	2
Cetoscarus ocellatus	6
Chaetodon	35
Chaetodon auriga	92
Chaetodon falcula	42
Chaetodon guttatissimus	233
Chaetodon kleinii	44
Chaetodon lunula	10
Chaetodon lunulatus	3
Chaetodon meyeri	63
Chaetodon striatus	82

Species	Number of thumbnails
Naso	3
Naso elegans	62
Nemanthias carberryi female	8
Nemanthias carberryi male	71
Nemateleotris magnifica	252
Novaculichthys taeniourus	2
Ostracion meleagris female	5
Oxymonacanthus longirostris	68
Paracirrhites forsteri	148
Parupeneus macronemus	3
Parupeneus trifasciatus	11
Plectorhinchus obscurus	40
Plectroglyphidodon dickii	229
Plectroglyphidodon johnstonianus	12
Plectroglyphidodon lacrymatus	105
Plectropomus laevis	11
Plectropomus punctatus	53
Pomacentrus	10
Pomacentrus caeruleus	14
Pseudanthias	628
Pseudanthias bicolor female	85
Pseudanthias squamipinnis female	843
Pseudanthias squamipinnis male	384
Pseudocheilinus hexataenia	23
Ptereleotris evides	30
Pterocaesio	4
Pterocaesio tile	174
Pygoplites diacanthus	148
Sargocentron	6
Sargocentron caudimaculatum	8
Sargocentron cornutum	13
Scaridae	41
Scarus	28
Scarus frenatus male	36
Scarus rubroviolaceus male	19
Scarus sordidus female	23
Serranidae	11
Stegastes	7
Stegastes pelicieri	28
Sufflamen bursa	22
Thalassoma	27
Thalassoma amblycephalum	30
Thalassoma amblycephalum juv	114

Species	Number of thumbnails
Thalassoma hardwicke	410
Thalassoma hardwicke female	1
Thalassoma hardwicke male	21
Thalassoma hebraicum	72
Thalassoma lunare	77
Variola louti	16
Zanclus cornutus	187
Chaetodon trifascialis	56
Chaetodon trifasciatus	268
Chaetodon ulietensis	14
Chaetodontidae	4
Chromis	152
Chromis atripectoralis OR Chromis viridis	5
Chromis lepidolepis	199
Chromis viridis	765
Chromis xanthura	36
Ctenochaetus	22
Ctenochaetus strigosus	2
Ctenochaetus truncatus	427
Ecsenius midas	28
Epinephelus	4
Epinephelus fasciatus	7
Epinephelus flavocaeruleus	11
Epinephelus rivulatus	7
Epinephelus tukula	5
Fistularia commersonii	10
Gnathodentex	16
Gnathodentex aureolineatus	122
Gomphosus caeruleus female	259
Gomphosus caeruleus male	272
Gracila albomarginata	22
Gunnellichthys monostigma	10
Halichoeres	13
Halichoeres hortulanus	67
Halichoeres hortulanus transitional	29
Hemigymnus fasciatus	98
Heniochus	16
Hologymnosus annulatus	11
Kyphosus	18
Kyphosus cinerascens	9
Kyphosus vaigiensis	1
Labrichthys unilineatus	19
Labridae	144

Species	Number of thumbnails
Labroides	7
Labroides dimidiatus	167
Lutjanus	11
Lutjanus bohar	11
Lutjanus gibbus	84
Macolor niger juv	8
Malacanthidae	2
Monotaxis grandoculis	30
Myripristis	20
Myripristis kuntee	68
Myripristis murdjan	11
Zebrasoma	15
Zebrasoma rostratum	283
Zebrasoma scopas	231
unknown fish	91

Table 1: B_{det} – 3367 frames

Species	Number of thumbnails
Abudefduf sparoides	3,068
Abudefduf vaigiensis	5,124
Acanthurus leucosternon	3,259
Acanthurus lineatus	1,008
Acanthurus tennentii	1,115
Acanthurus thompsoni	3,201
Aethaloperca rogaa	1,885
Amblyglyphidodon indicus	1,188
Balistapus undulatus	1,787
Caesio lunaris	1,147
Caesio xanthonota	2,817
Cephalopholis argus	1,991
Chaetodon auriga	2,134
Chaetodon guttatissimus	1,182
Chaetodon kleinii	1,378
Chaetodon trifascialis	5,234
Chaetodon trifasciatus	4,421
Cheilinus fasciatus	1,333
Chromis dimidiata	7,004
Chromis opercularis	1,525
Chromis ternatensis	3,640
Chromis viridis	1,425
Chromis weberi	4,977

Species	Number of thumbnails
Dascyllus trimaculatus	1,103
Gnathodentex aureolineatus	1,796
Gomphosus caeruleus female	3,178
Gomphosus caeruleus male	3,131
Halichoeres hortulanus	3,192
Hemigymnus fasciatus	2,285
Hemitaenichthys zoster	1,136
Labroides dimidiatus	2,329
Lutjanus bohar	1,246
Lutjanus bohar juv	1,588
Macolor niger	2,643
Macolor niger juv	1,334
Monotaxis grandoculis	2,045
Monotaxis grandoculis juv	1,848
Naso brevirostris	1,134
Naso elegans	7,345
Naso vlamingii	1,684
Odonus niger	1,168
Oxymonacanthus longirostris	2,553
Parupeneus macronemus	3,469
Plectroglyphidodon dickii	1,458
Plectroglyphidodon lacrymatus	2,497
Pomacanthus imperator	1,847
Pomacentrus sulfureus	5,409
Pseudanthias squamipinnis female	1,542
Pygoplites diacanthus	3,746
Sargocentron caudimaculatum	1,111
Sargocentron diadema	1,031
Scarus tricolor female	1,140
Thalassoma hardwicke	4,951
Thalassoma hebraicum	2,173
Zanclus cornutus	3,876
Zebrasoma scopas	4,970
calcareous	7,323
corals hard	9,500
corals soft	1,948
dark	5,068
macroalgae	1,730
sand	2,066
water blue	1,000
water surface	4,050

Table 2: **B_{id}** – 176,486 thumbnails